Issues associated with sound exposure experiments in tanks

Alec J. Duncan, Klaus Lucke, Christine Erbe, and Robert D. McCauley

Citation: Proc. Mtgs. Acoust. **27**, 070008 (2016); doi: 10.1121/2.0000280
View online: http://dx.doi.org/10.1121/2.0000280
View Table of Contents: http://asa.scitation.org/toc/pma/27/1
Published by the Acoustical Society of America

Proceedings of Meetings on Acoustics

Volume 27 http://acousticalsociety.org/

Fourth International Conference on the Effects of Noise on Aquatic Life

Dublin, Ireland

10-16 July 2016

Issues associated with sound exposure experiments in tanks

Alec J. Duncan, Klaus Lucke, Christine Erbe and Robert D. McCauley

Centre for Marine Science and Technology, Curtin University, Perth, WA, Australia;

a.j.duncan@curtin.edu.au, k.lucke@curtin.edu.au, c.erbe@curtin.edu.au, r.mccauley@curtin.edu.au

For practical reasons it is often necessary to carry out sound exposure experiments on marine animals in tanks or pools that may have dimensions ranging from less than one meter to a few tens of meters. The boundaries of such tanks are almost invariably highly reflective to underwater sound, resulting in a sound field that can vary spatially in unexpected ways, and in which the relationship between pressure and particle velocity is quite different from that in an animal's natural environment. In this paper a numerical simulation based on the finite difference method is used to illustrate these effects. The results show that, at frequencies below the tank's lowest resonant frequency, the particle velocity and pressure fields vary smoothly in space and with changes in frequency, but that both the ratio of the particle velocity to the pressure and the way in which their amplitudes vary with distance from the source are different than in a free-field situation. At frequencies above the lowest resonant frequency the particle velocity and pressure fields, and their ratio, vary rapidly both spatially and with changes in frequency. Experimental measurements of pressure and particle velocity in a tank agree qualitatively with these results.

Published by the Acoustical Society of America

 [DOI: 10.1121/2.0000280]

1. INTRODUCTION

It is common practice for auditory and other bioacoustic measurements to be made in tanks or pools as a way of providing a convenient and well-controlled test environment (e.g., Fay and Popper, 1999; Kastelein et al., 1992; Sisneros, 2016; Thomas and Kastelein, 1990). However, most tanks have boundaries that are highly reflective to sound, leading to an acoustic field within the tank that is very different to that in an open water (acoustic free-field) environment (Parvulescu, 1967, Gray et. al. 2016, Rogers et. al., 2016). It is therefore important that those making such measurements sufficiently understand these effects to be able to evaluate the implications for their experiments. This paper is intended to facilitate this understanding by providing visualizations of the way in which the sound pressure and particle velocity fields in tanks vary with position and frequency. We further discuss the ratio of particle velocity to sound pressure, because many studies infer one from the other based on a constant relationship, which is only valid in the far field, where sound propagates as plane waves. Especially in studies on animals which are sensitive to particle velocity (such as fish and invertebrates) it is imperative to understand this relationship well and measure the right metric in order to draw correct conclusions about sensitivities.

Visualizations were created for a typical rectangular and cylindrical tank using a numerical method that captures the essential characteristics of the acoustic field while remaining computationally efficient. The desire for computational efficiency made it necessary to treat the floor and walls of the tank using relatively simple boundary conditions and as a result the simulations used to create the visualizations are suitable for obtaining the general characteristics of the acoustic fields in tanks, but not for accurately predicting the acoustic field in a particular tank.

Because this paper is primarily directed towards bioacousticians, the body of the paper focuses on the characteristics of the acoustic fields as shown by the visualizations, and the presentation of the details of the simulations that were used to generate the visualizations is restricted to a brief outline in Appendix A.

Videos of the visualizations are available at youtu.be/aQx3QWbf5aI (rectangular tank), and youtu.be/EO4q_ua0Gbw (cylindrical tank), and are highly recommended as they provide a much better impression of how the fields vary with frequency than the static images contained in this paper.

2. THE ACOUSTIC FIELD IN A RECTANGULAR TANK

Figure 1 shows one frame of the visualization video for a 2.5 m long x 1.52 m wide x 1.28 m water depth rectangular tank. These dimensions were chosen to match those of a tank that is frequently used by the authors for acoustics experiments. The tank is open at the top, has thin steel sides, and is lined with a plastic pool liner which, at the bottom of the tank, is in direct contact with a concrete floor. For the purposes of the visualization the sound speed in the fresh water in the tank was assumed to be 1484 m/s, corresponding to the measured water temperature at the time of the comparison measurements described in Section 4. The boundary conditions were chosen so as to give a pressure reflection coefficient for normal incidence sound of 0.8 for the floor of the tank and -0.95 for the walls and water surface.

In Fig. 1, the top left plot shows a horizontal cross-section of the acoustic pressure in the tank at mid water depth at a frequency of 200 Hz, and the top right plot shows the magnitude of the

particle velocity over the same horizontal cross-section. The color scales of both these plots have dynamic ranges of 80 dB. The white dot is an acoustic source that, in open water, would produce a sound pressure level of 120 dB re 1 µPa at a range of 1 m. The motions of the radiating surfaces of the source were assumed to be unchanged by placing the source in the tank (see Appendix A for further details). The black dot shows the location of a receiver (hydrophone and particle velocity sensor), the output of which is plotted in the bottom three panels. Both source and receiver are at mid water depth, and the distance between them is 1 m. The solid blue lines in the bottom three panels show, from left to right, the sound pressure level in dB re 1 µPa, the magnitude of the particle velocity in dB re 1 m/s, and the ratio of the magnitude of the particle velocity to the sound pressure in dB re $1/Z_0$ (where Z_0 is the acoustic impedance of the water, i.e., the product of its density and sound speed), all as a function of frequency. The lowest frequency shown is 50 Hz and the highest frequency is that corresponding to the pressure and particle velocity cross-sections shown in the top two panels (200 Hz in Fig. 1). In each of these plots the red broken line shows the output of a receiver at the same distance from the source in open water. The higher open water particle velocity at low frequencies is due to the receiver being in the acoustic nearfield of the source at these frequencies (Kinsler et. al., 2000, section 5.11).

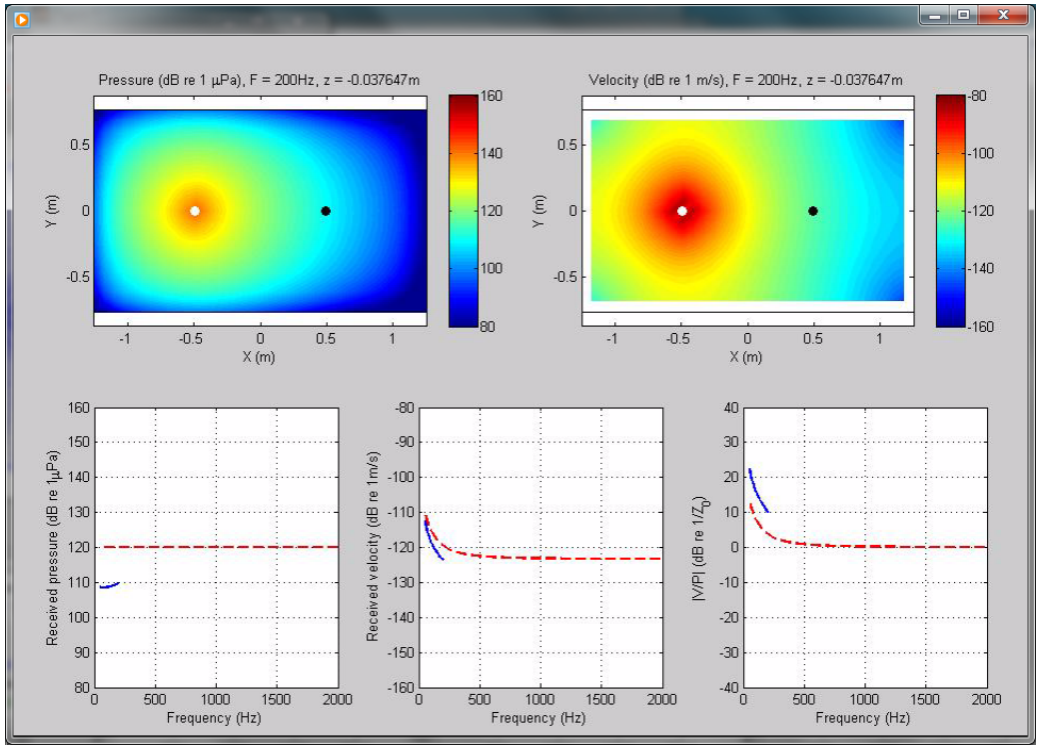

Figure 1. Rectangular tank visualization for a frequency of 200 Hz (top panels) and for frequencies between 50 and 200 Hz (blue lines, bottom panels).

Other selected frames from the same visualization are shown in Figures 2 to 6. These frames were chosen to highlight particular features of the way in which the acoustic field changes with frequency as discussed below. When considering these images it is important to bear in mind that they only show one horizontal cross-section of the acoustic field and that similar variations in pressure and particle velocity are occurring throughout the three dimensional volume of the tank. It is also important to note that the line plots are specific to the particular locations chosen for the source and receiver. Changing the location of source or receiver will lead to results that

differ from those shown here, but many qualitative similarities will remain. In particular the frequencies of the various resonances described below will be independent of the source and receiver location, but the pressures and particle velocities they produce at the receiver will depend on these locations.

At very low frequencies (Fig. 1), both the pressure and particle velocity fields vary smoothly within the tank, but the pressure at the receiver is some 10 dB lower than it would be at the same distance from the source in open water. The particle velocity is close to its open water value and the ratio of the particle velocity to pressure is approximately 10 dB higher than it would be in open water. As the frequency is increased (Fig. 2), the pressure initially increases towards its open water value, but then continues to increase, ultimately peaking when the frequency reaches the lowest resonant frequency of the tank, which in this case is 645 Hz (Fig. 3). The pressure maximum at the lowest frequency resonance occurs throughout the tank. At the receiver location chosen here the pressure peaks 20 dB higher than its open water value and there is also a particle velocity maximum at the same frequency, however, the ratio of particle velocity to pressure is lower than its open water value.

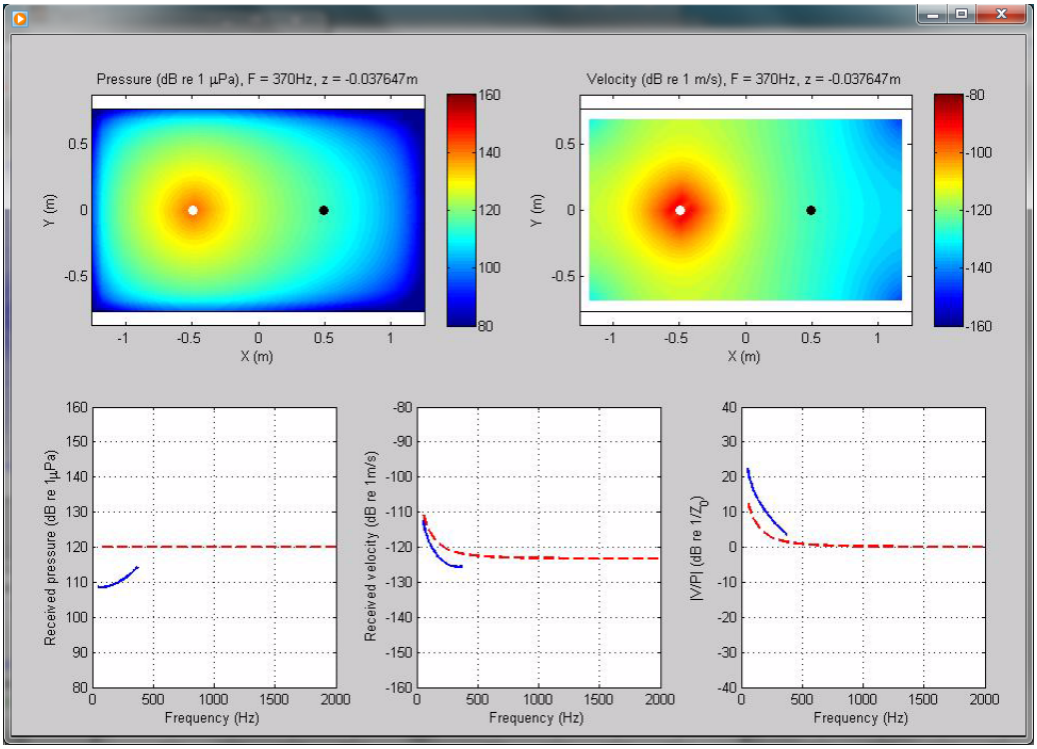

Figure 2. Rectangular tank visualization for a frequency of 370 Hz (top panels) and for frequencies between 50 and 370 Hz (blue lines, bottom panels).

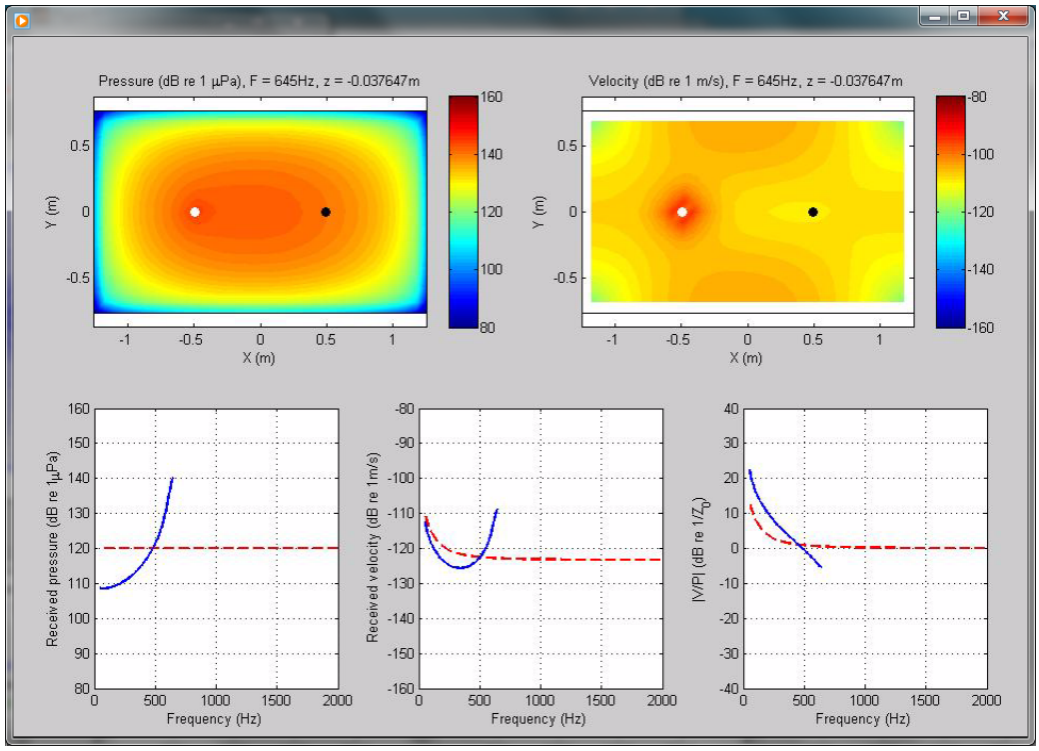

Figure 3. Rectangular tank visualization for a frequency of 645 Hz(top panels) and for frequencies between 50 and 645 Hz (blue lines, bottom panels).

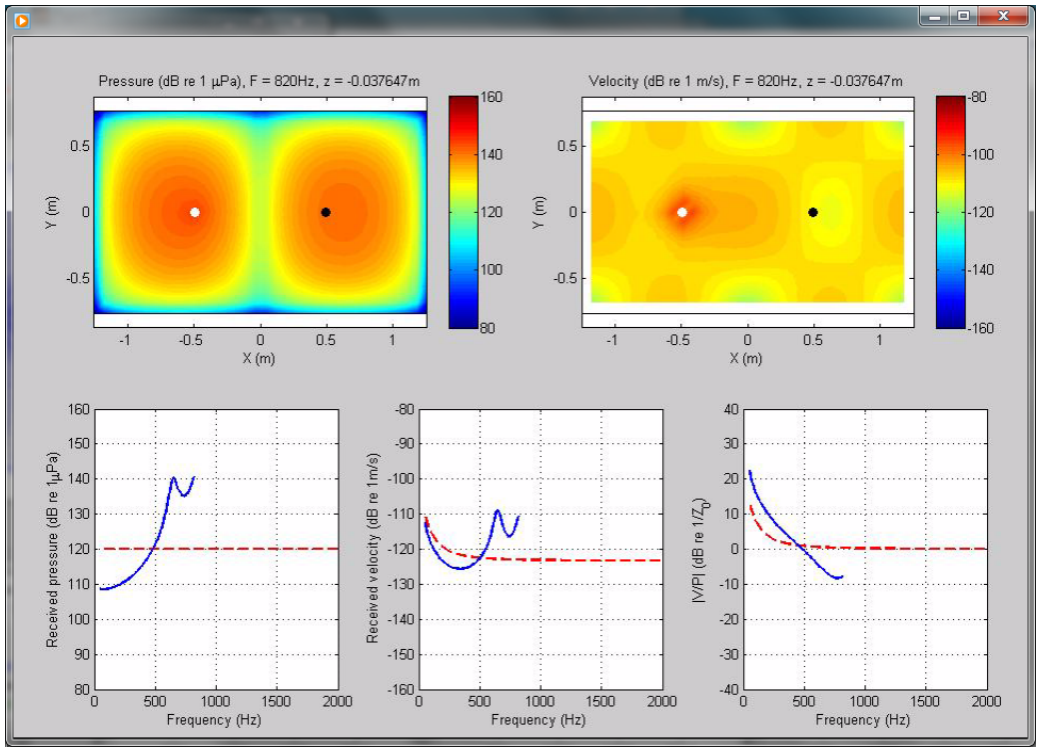

Figure 4. Rectangular tank visualization for a frequency of 820 Hz (top panels) and for frequencies between 50 and 820 Hz (blue lines, bottom panels).

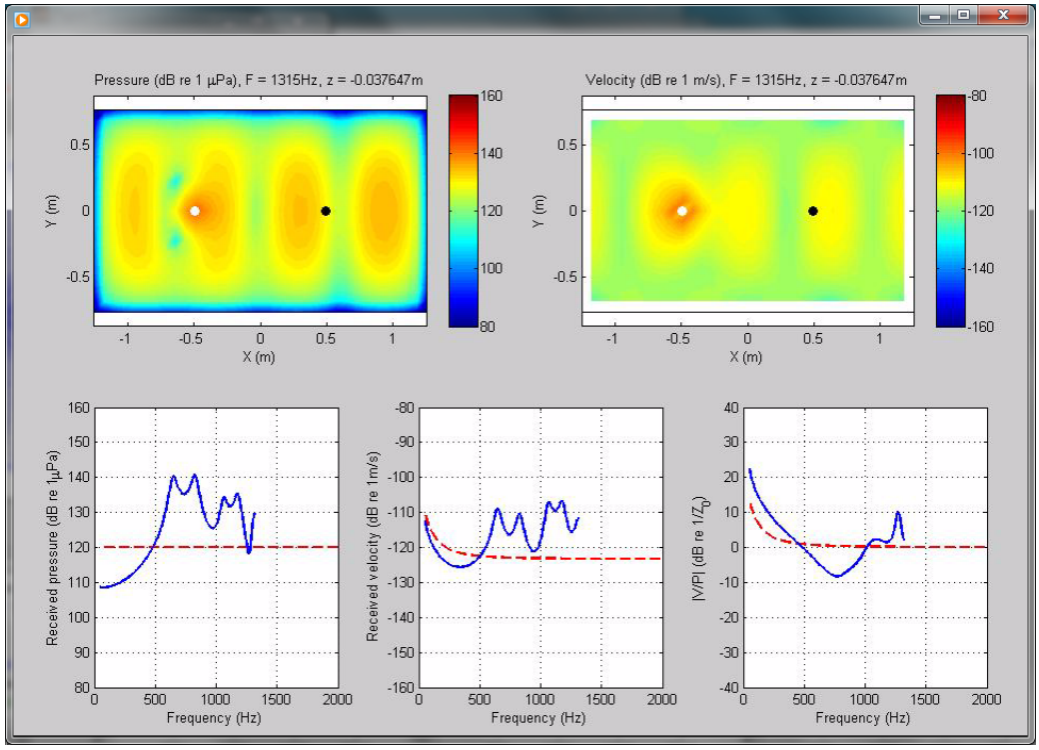

Figure 5. Rectangular tank visualization for a frequency of 1315 Hz top panels) and for frequencies between 50 and 1315 Hz (blue lines, bottom panels).

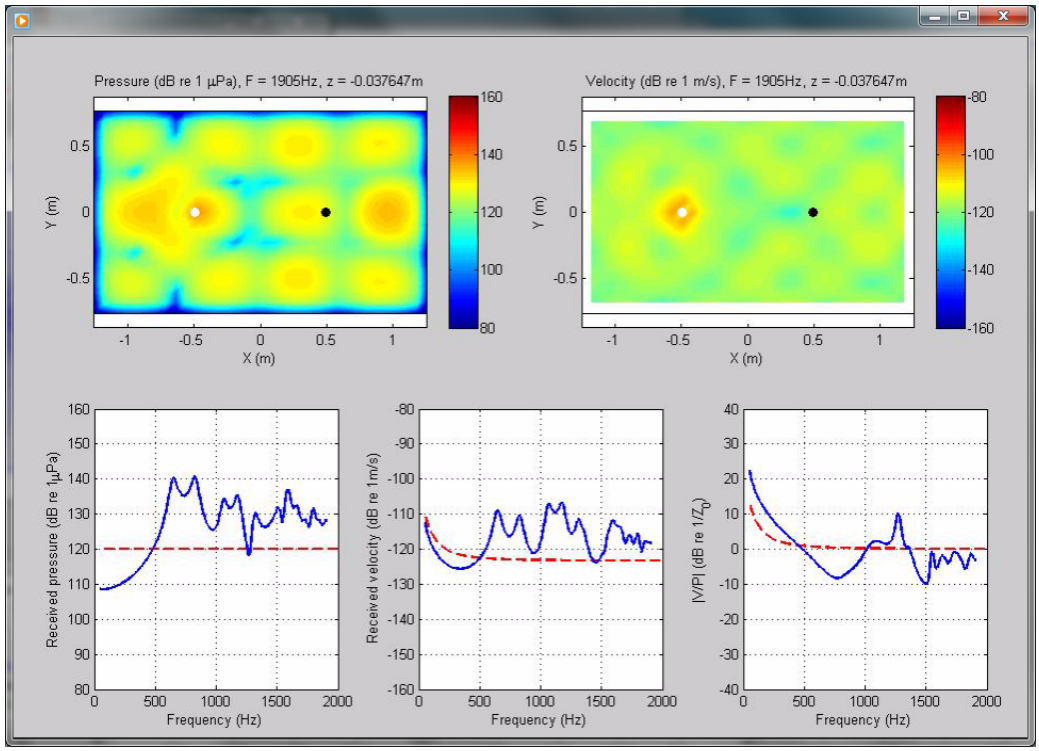

Figure 6. Rectangular tank visualization for a frequency of 1905 Hz (top panels) and for frequencies between 50 and 1905 Hz (blue lines, bottom panels).

As the frequency is increased further (Figs. 4 through 6) the received pressure and particle velocity go through a series of maxima and minima, and the particle velocity to pressure ratio varies between 10 dB above and 10 dB below its open water value. Many of these variations occur over quite small frequency ranges and they are accompanied by substantial changes in the spatial distributions of pressure and particle velocity.

3. THE ACOUSTIC FIELD IN A CYLINDRICAL TANK

Visualizations of the acoustic field in a cylindrical tank are presented in Figures 7 to 11 in a similar format to the rectangular tank visualizations presented in the previous section. The properties of this tank were again chosen to represent an actual experimental tank used by the authors. The tank is 2.5 m in diameter, has a water depth of 1.0 m, and being filled with seawater in quite a warm outdoor environment, the assumed sound speed was 1530 m/s. This tank was placed on a wooden platform that was expected to be acoustically soft, and so the boundary conditions for all boundaries were set to give a normal incidence pressure reflection coefficient of -0.95. The source and receiver are at mid water depth and are placed symmetrically, 1 m apart, on either side of the geometric center of the tank.

The white circle at the center of each particle velocity field plot is the result of a numerical difficulty in calculating the particle velocity at that point in cylindrical coordinates and has no physical significance.

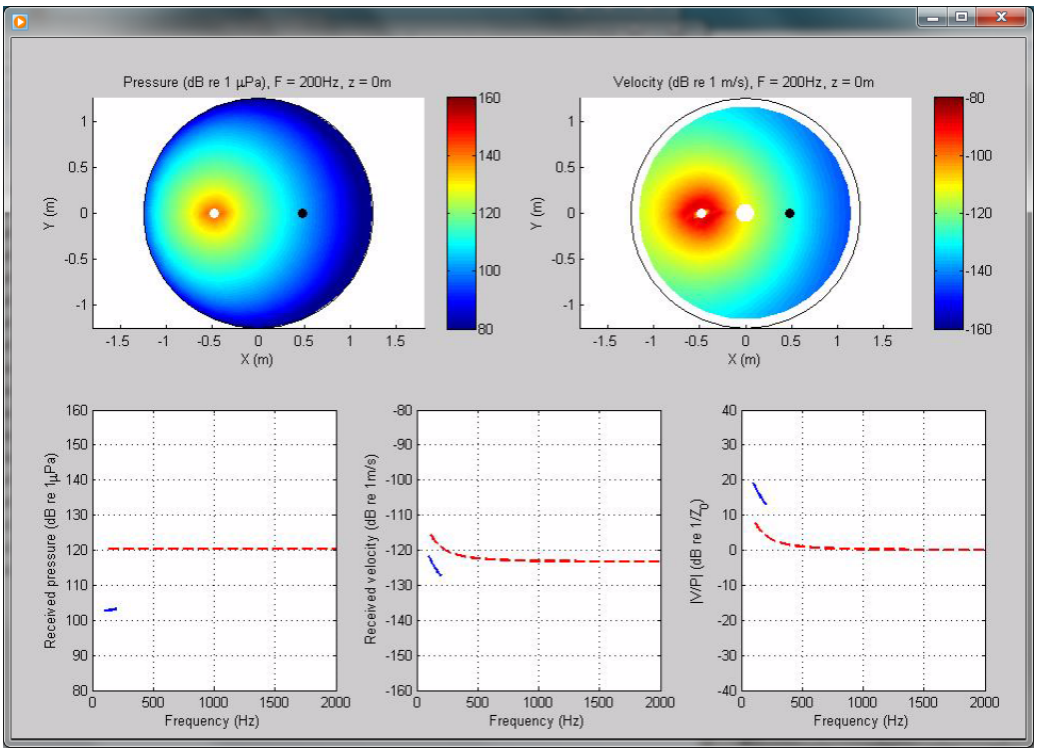

Figure 7. Cylindrical tank visualization for a frequency of 200 Hz (top panels) and for frequencies between 50 and 200 Hz (blue lines, bottom panels).

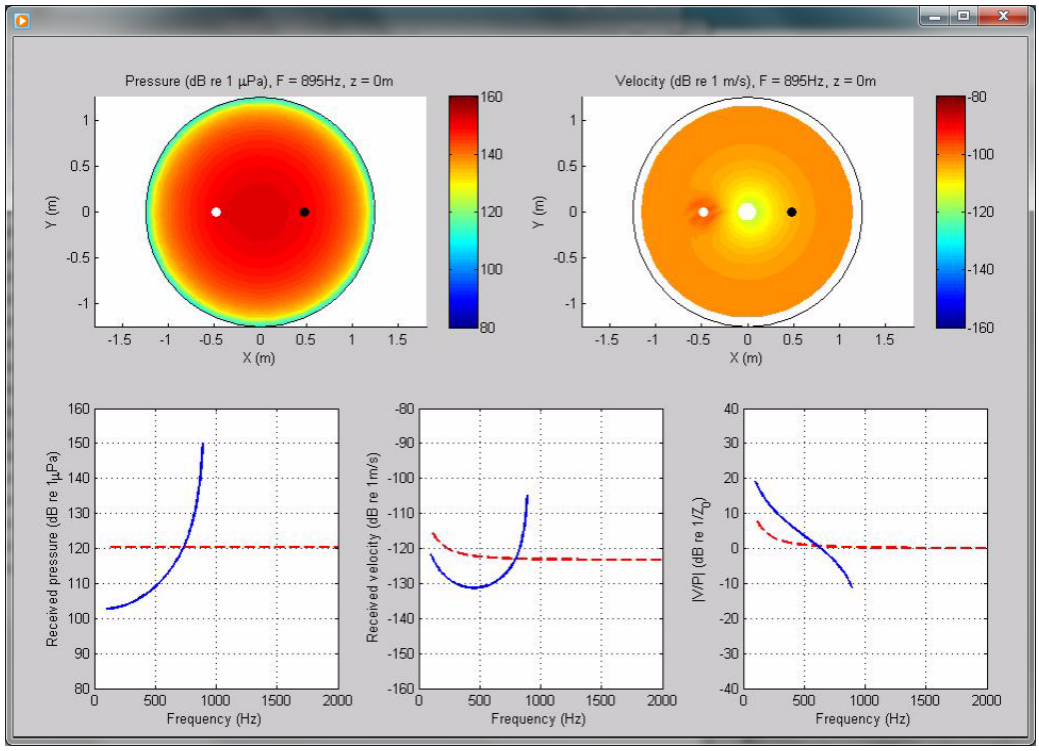

Figure 8. Cylindrical tank visualization for a frequency of 895 Hz (top panels) and for frequencies between 50 and 895 Hz (blue lines, bottom panels).

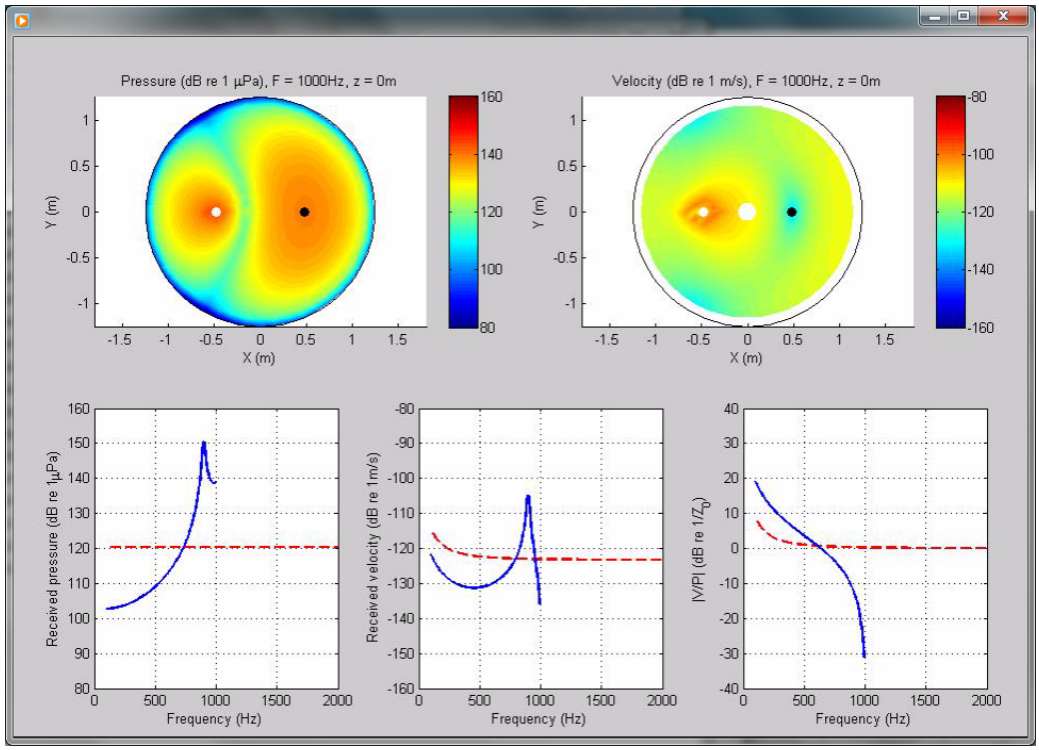

Figure 9. Cylindrical tank visualization for a frequency of 1000 Hz (top panels) and for frequencies between 50 and 1000 Hz (blue lines, bottom panels).

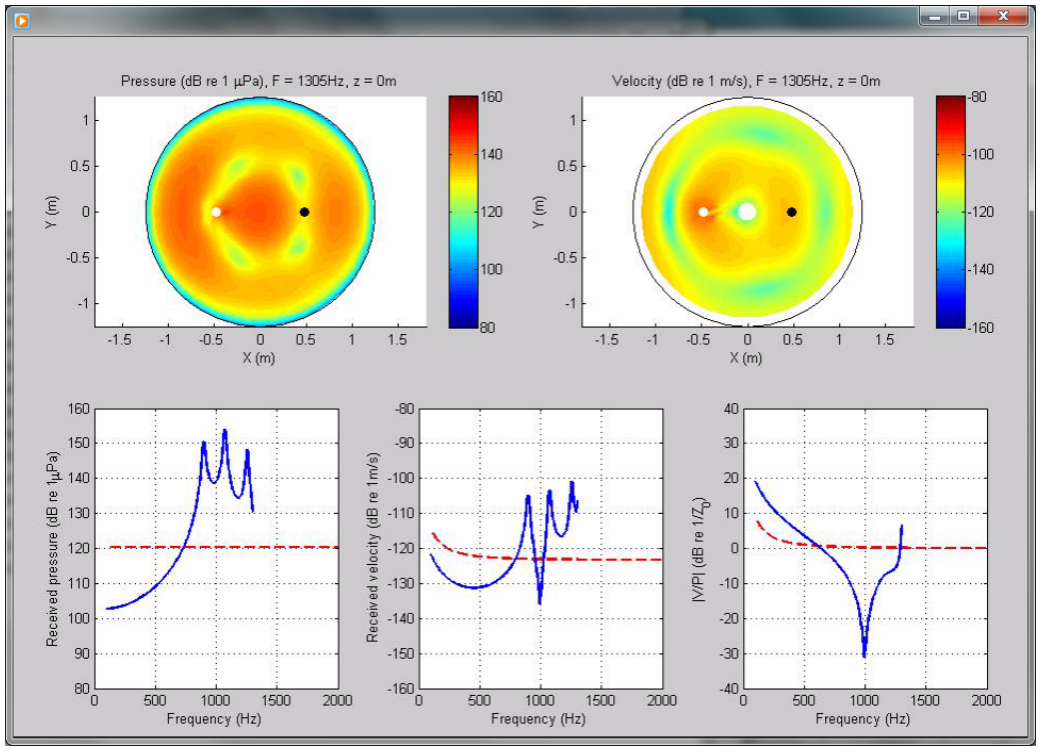

Figure 10. Cylindrical tank visualization for a frequency of 1305 Hz(top panels) and for frequencies between 50 and 1305 Hz (blue lines, bottom panels).

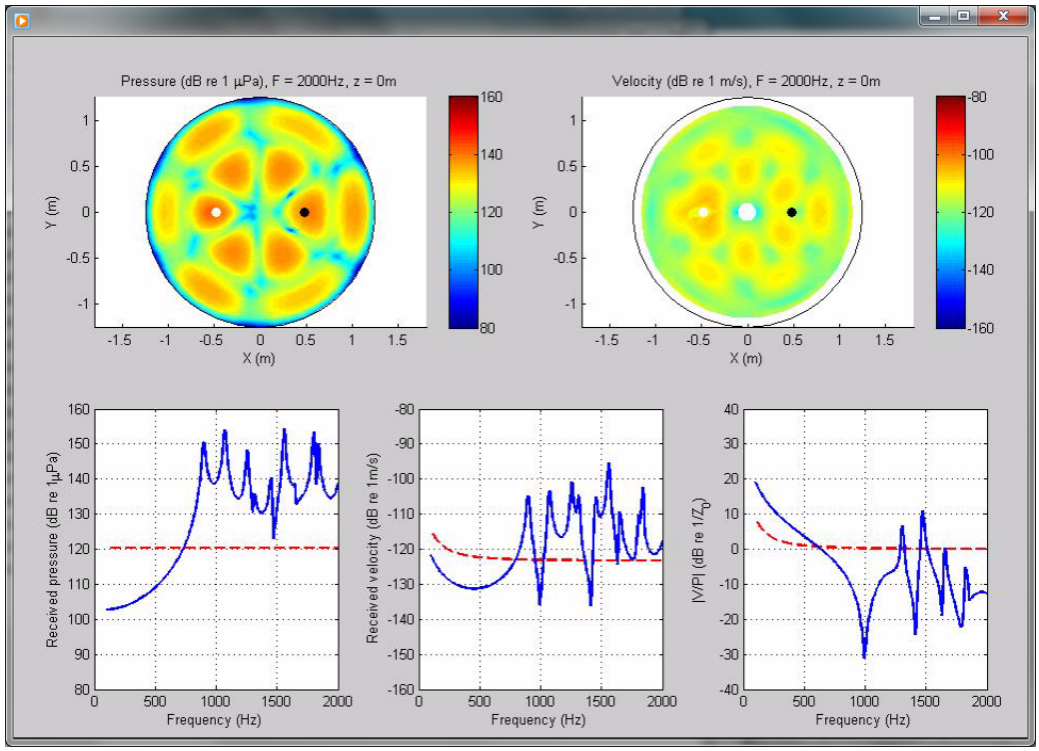

Figure 11. Cylindrical tank visualization for a frequency of 2000 Hz (top panels) and for frequencies between 50 and 2000 Hz (blue lines, bottom panels).

Apart from some obvious changes in the geometry of the acoustic field that are required to fit the cylindrical geometry of the tank, the way in which the acoustic field changes with frequency is very similar to the rectangular tank example given above. However, there are some noticeable differences:

- Although the diameter of the cylindrical tank is the same as the length of the rectangular tank, and the water depths are similar, the lowest resonant frequency of the cylindrical tank (895 Hz, Fig. 8) is much higher than that of the rectangular tank (645 Hz). This is the result of the assumption of an acoustically soft bottom boundary for the cylindrical tank rather than the acoustically hard bottom boundary assumed for the rectangular tank. Re-running the cylindrical tank simulation with the same bottom boundary condition used for the rectangular tank reduced the lowest resonant frequency to 630 Hz – very close to the rectangular tank value.
- The cylindrical tank visualization exhibits sharper resonances and larger changes (more than 30 dB) in pressure, particle velocity, and particle velocity to pressure ratio than the rectangular tank visualization. This is again due to the change in bottom boundary condition rather than the change in tank geometry. The energy loss per bottom refection is proportional to the square of the pressure reflection coefficient, so the pressure reflection coefficient of -0.95 used for the bottom of the cylindrical tank results in significantly less energy loss per bottom reflection than the value of +0.8 used for the rectangular tank, leading to the observed effects.

Figure 9 has been chosen to demonstrate a situation where the pressure at the receiver is high, but the particle velocity is at a minimum. At any particular frequency, the particle velocity is proportional to the spatial gradient of the pressure (Jensen et. al., 2011, section 2.1.2; Kinsler et. al., 2000, section 5.4) and at this frequency the receiver happens to be at a spatial maximum of the pressure field where the pressure gradient is very small. The converse situation is shown in Fig. 10 where there is a low pressure but a large spatial pressure gradient at the receiver, leading to a high particle velocity. The large pressure gradient is not obvious from Fig. 10 because it does not show the phase of the pressure field, however in this case the inner circular high pressure region and the outer ring of high pressure are 180° out of phase, so there is a large pressure gradient between them. Figure 11 shows the increasing complexity of the higher frequency resonances.

4. COMPARISON BETWEEN SIMULATION AND MEASUREMENT

In order to provide some confidence in the validity of the visualizations, the simulated pressure and particle velocity for the rectangular tank were compared with measurements carried out in the real tank described in Section 2 with the same source-receiver geometry used in the simulation.

The source was a Lubell LL-9162T underwater speaker, and the receiver was a GeoSpectrum M20 particle velocity sensor interfaced to a JASCO AMAR G3 digital recorder. The underwater speaker was driven via a power amplifier with a sinusoidal, swept frequency signal from a laboratory function generator. The frequency of the signal was swept linearly from 50 Hz to 3 kHz over 200 s. The voltage waveform across the terminals of the underwater speaker was measured using a using a digital oscilloscope. Data analysis was carried out with custom programs written in Matlab (The MathWorks Inc.). The manufacturer's calibration curve for the underwater speaker was used to convert the measured voltage to the expected free-field acoustic

pressure, and the corresponding free-field particle velocity was calculated from this based on the usual relationship between the pressure and particle velocity for a spherical wave (Kinsler et al., 2000, section 5.11). The measured pressures and particle velocities were referenced to these predicted free-field values.

The results are shown in Fig. 12 and demonstrate that, while there are large differences between predicted and measured levels at some frequencies, the simulation captures many of the features in the measured data, including the smooth increase in pressure up to the lowest resonant frequency, and the large variations in levels that occur above that frequency. The lowest two resonances are clearly visible in the measured data, as are a number of the higher frequency resonances, and although the measured and simulated resonant frequencies don't agree exactly, they are well within the accuracy expected from the simulation given its simplistic treatment of the boundary conditions.

5. DISCUSSION

The most important points to be drawn from these visualizations, together with a few additional insights from physical acoustics are as follows:

- Any tank will have a series of resonant frequencies. The frequencies of these resonances depend on the dimensions of the tank and the acoustic properties of the tank walls and floor. All else being equal, doubling all the linear dimensions of a tank will halve all the resonant frequencies and vice-versa.

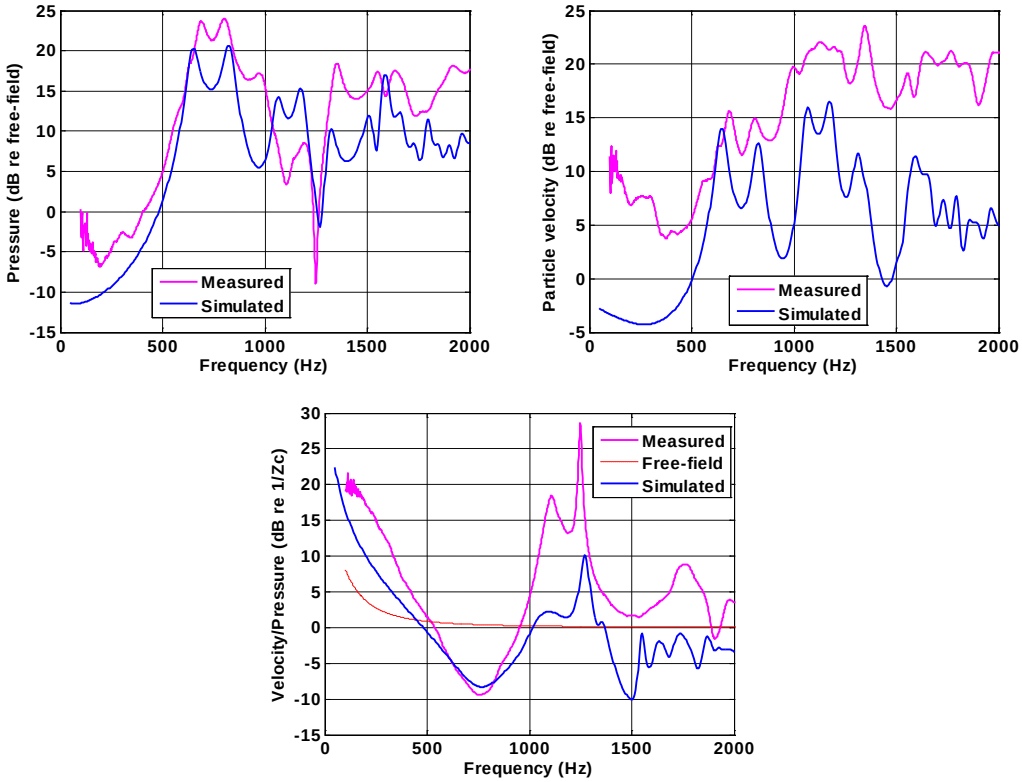

Figure 12. Cylindrical tank visualization for a frequency of 2000 Hz.

- In most cases the lowest resonant frequency of a rectangular tank with a free water surface will be somewhere between that of a tank with a rigid floor and walls, $f_0 = \frac{c}{4H}$, and that of a tank where all boundaries are acoustically soft, $f_0 = \frac{c}{2}\sqrt{\frac{1}{L^2}+\frac{1}{W^2}+\frac{1}{H^2}}$. Here f_0 is the resonant frequency (Hz), c is the sound speed (m/s), and L, W and H are respectively the tank's length, width and water depth (m). The lowest resonant frequency of a rectangular tank with a rigid floor and acoustically soft walls is: $f_0 = \frac{c}{2}\sqrt{\frac{1}{L^2}+\frac{1}{W^2}+\frac{1}{4H^2}}$.
- Similarly, the lowest resonant frequency of a cylindrical tank will usually be somewhere between the rigid floor and wall result, $f_0 = \frac{c}{4H}$, and the resonant frequency of a cylindrical tank with all acoustically soft boundaries, which can be shown to be $f_0 = \frac{c}{2}\sqrt{\frac{2.344}{D^2}+\frac{1}{H^2}}$, where D is the diameter of the tank (m). The lowest resonant frequency of a cylindrical tank with a rigid floor and acoustically soft walls is $f_0 = \frac{c}{2}\sqrt{\frac{2.344}{D^2}+\frac{1}{4H^2}}$.
- At frequencies well below the lowest resonant frequency the acoustic field will vary smoothly, both spatially and with changes in frequency, however both the pressure and particle velocity will be different from their values at the same distance from the same source in open water, and their ratio will also be different from that in open water.
- For frequencies approaching and above the lowest resonant frequency the sound field will change rapidly with changing frequency. Above the lowest resonant frequency it will also become increasingly complicated spatially.
- Although accurate quantitative prediction of the field in the tank at a given frequency is possible in principle, it is unusual for it to be practicable, even with a much more capable numerical model than the one used here, because of the dependence of the field on the detailed mechanical and acoustic properties of the tank boundaries, which are unlikely to be known with sufficient accuracy.
- Finally, the presence of animals in the tank can alter the acoustic fields again, in particular if their (or some of their organs' and tissues') acoustic impedance differs greatly from that of the surrounding water. This also occurs in open water, but the way in which the sound field in a tank will be modified by the presence of an animal will be different from the way in which the same animal will affect the sound field in open water.

6. CONCLUSION

These observations lead to the conclusion that it is essential to measure the acoustic field in any tank in which bioacoustics experiments are to be carried out, and that these measurements need to include both the frequency dependence and spatial dependence of the acoustic field. Working at frequencies well below the tank's lowest resonant frequency will result in an acoustic field that varies smoothly spatially, making it easier to characterise, and also providing a more uniform environment for bioacoustics experiments, however the field will not correspond to that generated by the same source in open water.

If an animal under test is known to only be sensitive to pressure, then pressure measurements would suffice, however if it is susceptible to particle velocity then all three components of the particle velocity vector need to be measured. Particle velocity can be measured directly with a

vector sensor, or indirectly via the pressure gradient. Determining a single particle velocity component by the pressure gradient method requires two accurately matched hydrophones in close proximity, and determining all three components requires either three sequential measurements with the two hydrophones in different relative positions, or a single measurement with an array of at least four hydrophones. The spacing between the hydrophones needs to be small compared to the acoustic wavelength, but not too small or the result will become sensitive to slight mismatches between the hydrophones.

The equations given in Section 5 provide some guidance as to the lowest resonant frequency of a tank of a particular size and shape; however there is typically a large uncertainty due to the uncertain boundary conditions, and the only way to accurately determine this frequency is to measure it. The fact that the pressure maximum occurs throughout the tank makes this a relatively easy measurement to do, as all that is required is a source somewhere in the tank and a hydrophone at a single location. The voltage across the source and the output of the hydrophone should be measured as a function of frequency and then the measured pressures should be corrected for the transmit response of the source prior to locating the resonance peak.

APPENDIX A

This appendix provides brief technical details of the simulations that were used to generate the visualizations described in this paper.

The visualizations were generated by two simulations written in the Matlab programming language; one for simulating rectangular tanks and the other for simulating cylindrical tanks. Both used the finite difference method (FDM) to solve the Helmholtz Equation for pressure (Jensen et al. 2011, sections 2.1 and 2.2), with the rectangular tank simulation solving the equation in rectangular coordinates and the cylindrical tank simulation solving it in cylindrical coordinates. The FDM is a well-established method for solving partial differential equations and there are numerous textbooks on the subject, for example Mitchell and Griffiths (1980), Morton and Mayers (2005). This method essentially approximates the partial differential equation and its boundary conditions as a set of difference equations, which can then be converted to a set of simultaneous equations and solved by conventional matrix techniques.

The boundary conditions for the walls, floor and surface of both the rectangular and cylindrical tank simulations were normal impedance boundary conditions. In other words, the ratio of the pressure to the component of the particle velocity normal to the boundary was defined on each boundary. At a given frequency the particle velocity is proportional to the spatial gradient of the pressure, allowing this relationship to be expressed as a difference equation in pressure for each grid point on the boundary, which was included in the set of simultaneous equations to be solved. The advantage of this form of boundary condition is that the same equations can be used for boundaries ranging from completely free (e.g. the water surface) to rigid (e.g. an infinitely hard floor). The normal impedance for each boundary was specified independently so as to achieve a desired pressure reflection coefficient for normally incident sound on all types of boundaries. Real tank boundaries are unlikely to conform well to a constant normal impedance model, which is the main limitation of the method used here.

The cylindrical tank simulation required an additional boundary condition that forced the pressure at a given depth at zero range on all tank radials (i.e. in the center of the tank) to have the same value. The Helmholtz Equation in cylindrical coordinates has a singularity at the tank center, so the pressure at this point was calculated as the average of the values at the immediately surrounding points.

The source was implemented as a small bounded region of the computational grid. The normal velocity on the surface of this region was chosen to achieve the volume velocity that would produce a root mean square (rms) pressure of 1 Pa (corresponding to a sound pressure level of 120 dB re 1 µPa rms) at a range of 1 m in open water (Kinsler et al. 2000, sections 7.1 and 7.2). The surface velocity was again related to the pressure gradient via the appropriate difference equation and included in the set of simultaneous equations.

The resulting set of equations is sparse, which means that when expressed in matrix form there are many more zero than non-zero elements in the coefficient matrix. It was found that using Matlab's sparse matrix type instead of a regular matrix to store the coefficients made the solution of the equations much faster, resulting in a simulation that takes less than 1 s to compute the three-dimensional pressure field at a single frequency in the rectangular tank at 7.5 cm resolution using a single core of a 2.8 GHz Intel i7 processor with 16 GBytes of RAM. The computational speed of the cylindrical tank simulation was similar. After the pressure field had been calculated, the velocity field was computed numerically from its spatial gradient.

REFERENCES

Fay, R. R., and Popper, A. N. (Eds.). (**1999**). *Comparative Hearing: Fish and Amphibians*. New York, NY: Springer Verlag.

Gray, M. D., Rogers, P. H., Popper, A. N., Hawkins, A. D., Fay, R. F. (**2016**). "Large Tank Acoustics: How Big Is Big Enough?", in *The Effects of Noise on Aquatic Life II*, edited by A. N. Popper, and A. D. Hawkins (Springer Science+Business Media, New York), pp. 363-369.

Jensen, F. B., Kuperman, W. A., Porter, M. B., Schmidt, H., (**2011**), *Computational Ocean Acoustics*, 2nd ed., (Springer Science+Business Media, LLC, New York), ISBN 9781441986771.

Kastelein, R. A., Supin, A. Y., and Thomas, J. A. (Eds.). (**1992**). *Marine Mammal Sensory Systems*. New York, NY: Springer Verlag.

Kinsler, L. E., Frey, A. R., Coppens, A. B., Sanders, J. V. (**2000**). *Fundamentals of Acoustics*, 4th ed., John Wiley & Sons, ISBN 9780471847892.

Mitchell, A. R. and Griffiths, D. F. (**1980**). *The finite difference method in partial differential equations*, (Wiley), ISBN: 0471276413.

Morton, K. W. and Mayers, D. F. (**2005**). *Numerical solution of partial differential equations: an introduction*, (Cambridge University Press), ISBN 0521607930.

Parvulescu, A. (**1967**). "The acoustics of small tanks", in: Tavolga WN (ed.) *Marine bioacoustics II*. (Pergamon, Oxford), pp. 7–13

Rogers, P. H., Hawkins, A. D., Popper, A. N., Fay, R. R., Gray, M. D. (**2016**). "Parvulescu revisited: small tank acoustics for bioacousticians", in *The Effects of Noise on Aquatic Life II*, edited by A. N. Popper, and A. D. Hawkins (Springer Science+Business Media, LLC, New York), pp. 933-941.

Sisneros, J. A. (**2016**). *Fish Hearing and Bioacoustics: An Anthology in Honor of Arthur N. Popper and Richard R. Fay*: Springer International Publishing.

Thomas, J. A., and Kastelein, R. A. (Eds.). (**1990**). *Sensory Abilities of Cetaceans: Laboratory and Field Evidence*. New York, NY: Springer Verlag.